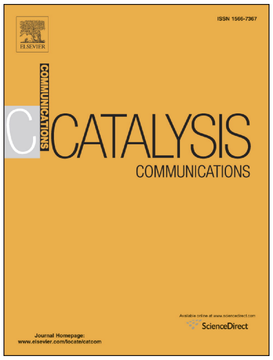

B-cation partial substitution of double perovskite La2NiTiO6 by Co2+: Effect on crystal structure, reduction behavior and catalytic activity

Pablo V. Tuza, Mariana M.V.M. Souza

PII: S1566-7367(17)30165-6
DOI: doi: 10.1016/j.catcom.2017.04.030
Reference: CATCOM 5015

To appear in: *Catalysis Communications*

Received date: 5 January 2017
Revised date: 12 April 2017
Accepted date: 15 April 2017

Please cite this article as: Pablo V. Tuza, Mariana M.V.M. Souza , B-cation partial substitution of double perovskite La2NiTiO6 by Co2+: Effect on crystal structure, reduction behavior and catalytic activity. The address for the corresponding author was captured as affiliation for all authors. Please check if appropriate. Catcom(2016), doi: 10.1016/j.catcom.2017.04.030

B-cation partial substitution of double perovskite La_2NiTiO_6 by Co^{2+}: effect on crystal structure, reduction behavior and catalytic activity

Pablo V. Tuza[1†] and Mariana M.V.M. Souza[1*]

[1] Escola de Química, Universidade Federal do Rio de Janeiro (UFRJ), Centro de Tecnologia, Bloco E, Sala 206, CEP 21941-909, Rio de Janeiro/RJ, Brazil

[†] Present address: Universidad Nacional de Loja, Carrera Químico Biológicas, Av. Pío Jaramillo Alvarado y Reinaldo Espinoza, sector La Argelia, Loja, Ecuador

* Corresponding author (Tel: 5521-39387598, Email: mmattos@eq.ufrj.br)

Abstract

$La_2NiTi_{0.9}Co_{0.1}O_6$ and $La_2Ni_{0.9}Co_{0.1}TiO_6$ perovskites were obtained by partial substitution of either Ti^{4+} or Ni^{2+} from double perovskite La_2NiTiO_6 by Co^{2+}. The Rietveld analysis demonstrated that all as-synthesized samples have orthorhombic symmetry and space group *Pbnm*. Quantitative phase analysis using Rietveld refinement of XRD profiles after temperature programmed reduction showed that the reduction of La_2NiTiO_6 was modified by partial substitution of either Ni^{2+} or Ti^{4+} by Co^{2+}, being more evident for the $La_2NiTi_{0.9}Co_{0.1}O_6$. The activity of all catalysts for steam reforming of methane was attributed to both the reduction degree of two-valence metals and the metal-support interaction.

Keywords: double perovskite, cobalt, nickel, quantitative phase analysis, reduction.

1. Introduction

Perovskites are oxides that can be represented by the formula ABO_3 [1], where A is a rare earth, alkali or alkaline earth metal and B is a transition metal [2]. Perovskite structure can be illustrated by B cations in the center of octahedra sharing corners, whose vertices are occupied by oxygen atoms (BO_6), and thus forming a framework that contains the A cations in the center of the cavities between layers of BO_6 octahedra. Double perovskites (DPs) are represented by the formula $A_2B'B''O_6$ [3] or $A'A''B'B''O_6$ [4] and the B-cation sublattice types known for DPs are rock salt, layered and random [4]. In rock salt ordering, $B'O_6$ and $B''O_6$ octahedra are ordered like Na and Cl atoms in NaCl structure. Layered ordering occurs when layers composed of either $B'O_6$ or $B''O_6$ octahedra are placed one above other. Random ordering is characterized by the absence of $B'O_6$ and $B''O_6$ octahedra sequence in the structure formed by octahedra sharing corners. Therefore, the rock-salt and layered present an ordered arrangement [4], which characterizes compounds known as ordered DPs.

DPs show interesting physical and chemical properties such as superconductivity, ferroelectricity, antiferroelectricity, piezoelectricity, magnetic properties and optical properties or a combination of both magnetic and electric interactions [5,6]. These materials have been used as electrode in fuel cells [7,8] as well as catalysts [9] and catalyst precursors [10].

The reduction of catalyst precursors is important for catalytic reactions because it is associated with the formation of metal active sites and the crystalline phases composing the support. Reducibility of cations varies according to its respective redox potential, *e.g.*, copper, nickel or cobalt are more difficult to reduce than iridium, rhodium or ruthenium, and can be modified by the neighboring anions in the crystalline structure since it is also influenced by the coordination number and precise location of the cations [11]. Concerning perovskites, the reduction of $LaNiO_3$ was well detailed in the literature [12,13]. The reduction of the La_2NiTiO_6 DP was reported in our previous work, as well as its catalytic activity for steam reforming of methane [14].

To the best of our knowledge, the influence of partial substitution of B-cations of the La_2NiTiO_6 DP has not been studied yet. Therefore, the main objective of this work is to partially substitute either Ti^{4+} or Ni^{2+} from La_2NiTiO_6 by Co^{2+} for obtaining $La_2NiTi_{0.9}Co_{0.1}O_6$ and $La_2Ni_{0.9}Co_{0.1}TiO_6$ perovskites, respectively, and then to evaluate the crystal structure after synthesis, crystalline phases after reduction and the catalytic activity of the prepared samples.

2. Experimental

2.1. Synthesis

$La_2NiTi_{0.9}Co_{0.1}O_6$ ($LNT_{0.9}Co_{0.1}O$), $La_2Ni_{0.9}Co_{0.1}TiO_6$ ($LN_{0.9}Co_{0.1}TO$) and La_2NiTiO_6 (LNTO) were prepared by modified Pechini method [15]. Steps related to citrate and the preparation of the polyester solution with subsequent resin formation and its calcination were detailed in our previous work [14]. The weak sponge-like structure obtained was mixed and ground in agate mortar, calcined in air at 800 °C for 17 h with a heating rate of 10 °C min^{-1}, and finally milled again.

2.2. Characterization

Chemical composition of the materials was determined by X-ray fluorescence (XRF) using a Rigaku Primini spectrometer and expressed on the basis of the amount of cations in each sample. Crystalline phases of as-synthesized samples and the materials after temperature programmed reduction were determined by means of X-ray diffraction (XRD), using a Rigaku Miniflex II X-ray diffractometer equipped with a graphite monochromator and CuKα radiation (30 kV and 15 mA). The measurements were carried out over the 2θ range of 5-90°, step size equal to 0.05°, and a counting time of 1 s per step. The identification of the crystalline phases was performed using crystallographic information files from Inorganic Crystal Structure Database (ICSD) and the collection code.

Average crystallite size was determined by Scherrer equation, using the full width at half maximum of the (112) or (111) diffraction peaks for the as-synthesized materials (2θ equal to 32.3°) or after temperature programmed reduction (2θ equal to 44.5°), respectively.

In order to refine the structure of the as-synthesized samples and to perform quantitative phase analysis (QPA) for each perovskite after temperature programmed reduction, it was carried out a Rietveld refinement of the corresponding XRD patterns using the Fullprof Suite Program 3.0 (version Febraury-2015) [16]. Details of the Rietveld refinement are provided on Supplementary Material.

Magnetic measurements as function of temperature for the LNTO sample, either in the zero-field cooled or in field cooled mode, were conducted using a cryogenic superconducting quantum interference device (SQUID) magnetometer, MPMS Quantum design model, in the temperature range 2-250 K, applying a magnetic field of 0.01 T. The molar susceptibility χ_m was calculated on the basis of the sample mass and the molecular weight.

Temperature programmed reduction (TPR) was performed in a microflow quartz-tube reactor operating at atmospheric pressure, using a sample amount equal to 1400 mg. This great amount of sample was used in order to distinguish the TPR peaks and variations of the baseline during isothermal period. The first step consisted in dehydration at 150 °C for 60 min under flowing Ar. The another step was the sample reducing with a flow rate of 55 mL min^{-1} of 10 % H_2/Ar, from room temperature to 1000 °C, coupled to an isothermal period at 1000 °C until the stabilization of the baseline, which occurred at 330 min. The outflowing gases were detected by thermal conductivity detector (TCD).

2.3 Catalytic tests

Catalytic activity for steam reforming of methane was evaluated in a fixed bed continuous flow reactor operated at atmospheric pressure. Initially, 50 mg of catalyst was reduced in situ with 150 mL min^{-1} of 10 % H_2/N_2 at 1000 °C for 2 h. The reaction was carried out with a total flow rate equal to 100 mL min^{-1} of 9.8 % CH_4/He and steam, which was introduced into the reactor through a water saturator at 43.7 °C under flowing CH_4/He. The reaction was performed in the temperature range 450-950 °C and H_2O/CH_4 molar ratio of 1:1. Analysis of reaction products was carried out in a Shimadzu gas chromatograph, with Carboxen 1010 Plot column, thermal conductivity and flame ionization detectors. CO and CO_2 were separated in the column and converted to CH_4 with a methanizer operating at 400 °C previous to detection by the flame ionization detector.

3. Results and discussion

Table 1 indicates the chemical composition of the as-synthesized materials determined by XRF. These values are close to nominal values, indicating appropriate application of the synthesis method.

Diffraction patterns and Rietveld analysis and of the as-prepared samples are presented in Fig. S1 of the Supplementary Material. The structural parameters, cell volumes, R-factors and chi squared values are shown in Table S1. The average crystallite sizes are smaller than 36 nm, which shows nanostructured materials. The lattice parameters of these materials are in accordance with the values reported for $LaNi_{0.5}Ti_{0.5}O_3$. In the case of the $LN_{0.9}Co_{0.1}TO$ and LNTO, metal to oxygen bond distances are similar to the corresponding from $LaNi_{0.5}Ti_{0.5}O_3$. In relation to the $LNT_{0.9}Co_{0.1}O$, although Ni/Ti/Co-O2 and Ni/Ti/Co-$O_{average}$ are close to values reported for $LaNi_{0.5}Ti_{0.5}O_3$, Ni/Ti/Co-O1 bond distances are different to the corresponding calculated from the crystallographic data of $LaNi_{0.5}Ti_{0.5}O_3$.

The larger difference between atomic radii of Ti^{4+} (0.605 Å, [17]) and Co^{2+} (0.745 Å, [17]) in $LNT_{0.9}Co_{0.1}O$ when compared to the corresponding from Ni^{2+} (0.69 Å, [17]) and Co^{2+} in the

$LN_{0.9}Co_{0.1}TiO$ could be related to the variation of the Ni/Ti/Co-O1 bond distances (Table S1). In fact, the exchange of Ti^{4+} from ordered DP La_2NiTiO_6 by a cation with significantly different atomic radii can affect the titanium to oxygen bond distances. For example, Yang *et al.* [18] reported that after substitution of Ti^{4+} from La_2NiTiO_6 by Mn^{4+} (atomic radius: 0.530 Å, [18]) in 0.2 mol, the six Ti-O bond distances of La_2NiTiO_6 (ICSD: 186433) were different to the corresponding of $La_2NiMn_{0.2}Ti_{0.8}O_6$ (ICSD: 186432).

According to the XRD patterns of Co^{2+}-containing materials, the absence of segregated phases points that an isomorphic partial substitution of either Ni^{2+} or Ti^{4+} from LNTO by Co^{2+} in 0.1 mol was achieved, which was confirmed by Rietveld refinement (Fig. S1a and S1b of Supplementary Material). Therefore, Co^{2+} atoms are included in the LNTO structure by partial substitution of either Ti^{4+} or Ni^{2+}. Moreover, all as-synthesized samples showed orthorhombic symmetry and space group *Pbnm*, and for the LNTO a random type arrangement of B-cations octahedra was obtained, according to the classification of DPs reported by Anderson *et al.* [4].

The evolution of the $\chi_m T$ values with temperature for the LNTO sample (Fig. S2 of Supplementary Material) indicates an antiferromagnetic behavior [19,20], with Néel temperature around 91 K, which agrees with the value of 100 K reported by Rodríguez *et al.* [20] for the same material with orthorhombic symmetry and space group *Pbnm*. Therefore, magnetic measurements corroborate the symmetry and space group of LNTO found by the Rietveld method.

Fig. 1 shows TPR profiles of the as-prepared samples performed from room temperature up to 1000 °C. Peaks at low temperature are related both to the reduction of Ni^{3+} to Ni^{2+} and the reaction between hydrogen from the mixture and adsorbed oxygen. The presence of Ni^{3+} species and adsorbed oxygen was found from XPS studies reported by Yang *et al.* [21] for $LaNi_{0.5}Ti_{0.5}O_3$ perovskite. Peaks at high temperature are associated with the reduction of Ni^{2+} and Co^{2+} in the crystalline structure to either Ni^0-Co^0 or Ni^0 (for the Co^{2+}-free DP). It is worth mentioning that Co^0 atoms were assumed to enter in the crystal lattice of Ni^0 (ICSD: 53807), and thus forming a Ni^0-Co^0 alloy (Fig. 2a and 2b). The reduction proceeds by reaction between lattice oxygen, bonded with either Ni^{2+} or Co^{2+}, and hydrogen from the mixture. Migration of either Ni^0-Co^0 for cobalt-containing materials or Ni^0 for LNTO from the structure is coupled to segregation of A-site species, like La_2TiO_5 and La_2O_3. These crystalline phases are in accordance with XRD patterns of the materials either after TPR (Fig. 2a-2c) or after reduction before reaction (RBR) (Fig. S3a-S3c of Supplementary Material), and with the reduction pathway reported by Arrivé *et al.* [22].

The isothermal period of TPR (Fig. 1) indicates different reduction behavior of each sample, as observed in the variation of the baseline. Ni^{2+} and Co^{2+} reduction degree to Ni^0-Co^0 or Ni^0 (in the case of LNTO), related to hydrogen consumption from the peak at high temperature and the isothermal period at 1000 °C, is shown in Table 1 for each sample. Reduction behavior for each sample was established by calculating the reduction degree which directly depends on the area of both the second reduction peak and the isothermal period. The integration method (IM), which calculates the area from any region under the TPR profile, was used instead of the deconvolution method for two reasons: (i) as shown in our last work for the case of the TPR of the La_2NiTiO_6 sample carried out with 10 % H_2/Ar [14], the reduction degree obtained from the area calculated by IM of the peak at 992 °C agrees with the reduction degree obtained from Rietveld refinement of the XRD pattern of the same sample after the TPR peak at 992 °C, indicating that the IM is a valid method to obtain the area of each TPR peak, and, (ii) considering that deconvolution method is more appropriate to obtain a peak area, the IM is adequate to obtain the area under the curve for the isothermal period because this area tends to be a rectangle rather than a peak. These values of reduction degree (more than 100 %) indicate additional hydrogen consumption in relation to the required quantity to reduce all the nickel and cobalt species contained in the samples. This increase in the expected hydrogen uptake could be related to the reduction of NiO and CoO formed by oxidation of either Ni^0-Co^0 with water vapor in the case of Co^{2+}-containing perovskites or NiO from oxidation of Ni^0 for LNTO. The presence of steam through the bed is associated with the low gas flow rates used for TPR [23], which could be favored by the large amount of sample used in this analysis.

Fig. 2 shows the Rietveld refinement of XRD profiles of the materials after TPR. Concerning Co^{2+}-containing perovskites, the calculated XRD profile of Ni^0-Co^0 was obtained by modifying the crystallographic information file of Ni^0 (ICSD: 53807) with occupation number values for Ni^0 and Co^0 proportional to Ni^{2+} and Co^{2+} content in the precursor.

After TPR, mass content of La_2TiO_5, Ni^0-Co^0 (or Ni^0 in the case of LNTO), La_2O_3 and the non-stoichiometric precursor are different for each sample, as shown in Table 1. The reduction degree of Ni^{2+} and Co^{2+} to Ni^0-Co^0 or Ni^{2+} to Ni^0 (for the case of LNTO) of the samples after TPR was 80.8 %, 86.7 % and 97.1 % for $LNT_{0.9}Co_{0.1}O$, $LN_{0.9}Co_{0.1}TO$ and LNTO, respectively (Table 1). This is according to the reduction degree of the same cations for each perovskite after RBR (Table S2 of supplementary data). Thus, the reduction of the LNTO is modified by substitution of either Ni^{2+} or Ti^{4+} by Co^{2+}. Also, the average crystallite sizes of Ni^0-Co^0 or Ni^0 obtained after TPR (42.3-31.1 nm, Table 1) are in accordance with the values of Ni crystallites sizes in the range 5-50 nm obtained by reduction of the $La_{0.5}Sr_{0.5}Ti_{0.75}Ni_{0.25}O_{3-\delta}$ perovskite [22].

The activity of these materials for steam reforming of methane ($CH_4 + H_2O \rightarrow 3H_2 + CO$) was investigated, and the results are displayed in Fig. 3. $LN_{0.9}Co_{0.1}TO$ and LNTO presented similar methane conversions over the whole temperature range, with activity from 550 ^oC. On the other hand, $LNT_{0.9}Co_{0.1}O$ showed much lower activity, with initial methane conversion only at 750 ^oC. The activity of $LN_{0.9}Co_{0.1}TO$ and LNTO catalysts can be related to their similar reduction degree after RBR (87.7 % and around 100 % for the perovskite where Ni^{2+} was substituted by Co^{2+} and the unsubstituted perovskite, respectively, Table S2 of Supplementary Material). On the other hand, the low activity of $LNT_{0.9}Co_{0.1}O$ can be attributed to the low reduction degree after RBR (39.1 %, Table S2 of Supplementary Material). It is worth noting that the reduction degrees for the perovskites after RBR can be correlated to those observed after TPR, with the same tendency (Table 1). The performance of each catalyst for the reaction can also be attributed to metal-support interaction, since Ni^0-Co^0 from $LN_{0.9}Co_{0.1}TO$ or Ni^0 from LNTO are mainly supported on La_2TiO_5, while Ni^0-Co^0 sites are principally supported on $LNT_{0.9}Co_{0.1}O$ non-s and La_2O_3. Related to the

$LNT_{0.9}Co_{0.1}O$, similar activity was found when compared to La_2NiTiO_6 reduced with 1.8 % H_2/Ar, whose performance was attributed to the reduction degree equal to 37.6 %, being the Ni sites supported on non-stoichiometric La_2NiTiO_6 and La_2O_3 [14]. The stability of these catalysts during heating (from 450 to 950 ^{o}C) and cooling (from 950 to 450 ^{o}C) cycle is reported on Supplementary Material. H_2/CO ratio close to stoichiometric value of 3 was obtained for all three catalysts at temperatures higher than 850 ^{o}C. At lower temperatures the H_2/CO ratio is higher than that expected for steam reforming of methane, due to the influence of shift reaction ($CO + H_2O \rightarrow CO_2 + H_2$), which is favored at low temperatures [24].

4. Conclusions

$La_2NiTi_{0.9}Co_{0.1}O_6$, $La_2Ni_{0.9}Co_{0.1}TiO_6$ and La_2NiTiO_6 were synthesized by modified Pechini method. Rietveld refinement of XRD patterns of the samples indicated orthorhombic symmetry and space group *Pbnm* for all as-synthesized samples, as well as the isomorphic partial substitution of Ni^{2+} or Ti^{4+} from La_2NiTiO_6 by Co^{2+}, and the random ordering of B-cations of the La_2NiTiO_6. Also, magnetic measurements corroborate the symmetry and space group of the double perovskite where B-cations are Ni^{2+} and Ti^{4+}. Quantitative phase analysis using the Rietveld refinement of XRD patterns of the perovskites after TPR showed that partial substitution of Ni^{2+} or Ti^{4+} by Co^{2+} modified the reduction of the Co^{2+}-free material. Moreover, $La_2Ni_{0.9}Co_{0.1}TiO_6$ and La_2NiTiO_6 presented higher catalytic activity for steam reforming of methane at temperatures between 450-750 °C. Furthermore, a higher onset temperature of 750 °C was observed for the reaction catalyzed with $La_2NiTi_{0.9}Co_{0.1}O_6$. The performance for the steam reforming of methane of all catalysts was correlated with the reduction degree and the metal-support interaction.

Acknowledgments

The authors thank Carlos André de Castro Perez from NUCAT/PEQ/COPPE/UFRJ for suggestions of Rietveld analysis. Also, they are grateful to Professor Alexandre Novak and Jilder Peña Serna from Laboratory of Low Temperatures at Physics Institute of the Federal University of Rio de Janeiro and Geraldo Cernicchiaro from Brazilian Center for Research in Physics for the magnetic measurements and data treatment. Pablo V. Tuza acknowledges to Secretaría de Educación Superior, Ciencia, Tecnología e Innovación SENESCYT-Ecuador for the financial support of this work.

References

[1] J.C. Pérez Flores, C. Ritter, D. Pérez-Coll, G.C. Mather, F. García-Alvarado, U. Amador, Synthesis, structures and electrical transport properties of the $La_{2-x}Sr_xNiTiO_{6-\delta}$ ($0 \leq x \leq 0.5$) perovskite series, J. Mater. Chem. 21 (2011) 13195-13204.

[2] T.K. Mandal, M. Greenblatt, Transition Metal Oxides: Magnetoresistance and Half-Metallicity, in: D.W. Bruce, D. O'Hare, R.I. Walton (Eds.), Functional Oxides, Wiley, Padstow, 2010, pp. 257–293.

[3] Y.P. Liu, S.H. Chen, H.R. Fuh, Y.K. Wang, First-principle calculations of half-metallic double perovskite $La_2BB'O_6$ (B,B'=3d transition metal), Commun. Comput. Phys. 14 (2013) 174–185.

[4] M.T. Anderson, K.B. Greenwood, G.A. Taylor, K.R. Poeppelmeier, B-Cation Arrangements in Double Perovskites, Prog. Solid State Chem. 22 (1993) 197–233.

[5] R. Shaheen, J. Bashir, Ca_2CoNbO_6: A new monoclinically distorted double perovskite, Solid State Sci. 12 (2010) 1496–1499.

[6] A. Ezzahi, B. Manoun, A. Ider, L. Bih, S. Benmokhtar, M. Azrour, M. Azdouz, J.M. Igartua, P. Lazor, X-ray diffraction and Raman spectroscopy studies of $BaSrMWO_6$ (M=Ni, Co, Mg) double perovskite oxides, J. Mol. Struct. 985 (2011) 339–345.

[7] C. Li, W. Wang, N. Zhao, Y. Liu, B. He, F. Hu, C. Chen, Structure properties and catalytic performance in methane combustion of double perovskites $Sr_2Mg_{1-x}Mn_xMoO_{6-\delta}$, Appl. Catal., B 102 (2011) 78–84.

[8] Z.Q. Deng, J.P. Smit, H.J. Niu, G. Evans, M.R. Li, Z.L. Xu, J.B. Claridge, M.J. Rosseinsky, B Cation Ordered Double Perovskite $Ba_2CoMo_{0.5}Nb_{0.5}O_{6-\delta}$ As a Potential SOFC Cathode, Chem. Mater. 21 (2009) 5154–5162.

[9] K.D. Campbell, Layered and double perovskites as methane coupling catalysts, Catal. Today 13 (1992) 245–253.

[10] Y.-H. Huang, G. Liang, M. Croft, M. Lehtimäki, M. Karppinen, J.B. Goodenough, Double-Perovskite Anode Materials Sr_2MMoO_6 (M = Co, Ni) for Solid Oxide Fuel Cells, Chem. Mater. 21 (2009) 2319–2326.

[11] P. Gallezot, Preparation of Metal Clusters in Zeolites, in: H.G. Karge, J. Weitkamp (Eds.), Post-Synthesis Modification I, Springer, Germany, 2003, pp. 257–306.

[12] T. Maneerung, K. Hidajat, S. Kawi, $LaNiO_3$ perovskite catalyst precursor for rapid decomposition of methane: Influence of temperature and presence of H_2 in feed stream, Catal. Today 171 (2011) 24–35.

[13] H. Provendier, C. Petit, A. Kiennemann, Steam reforming of methane on $LaNi_xFe_{1-x}O_3$ ($0 \leq x \leq 1$) perovskites. Reactivity and characterisation after test, C. R. Acad. Sci., Ser. IIc: Chim. 4 (2001) 57–66.

[14] P.V. Tuza, M.M.V.M. Souza, Steam Reforming of Methane Over Catalyst Derived from Ordered Double Perovskite: Effect of Crystalline Phase Transformation, Catal. Lett. 146 (2015) 47–53.

[15] M.M. Vijatović, J.D. Bobić, B.D. Stojanović, History and challenges of barium titanate: Part I, Sci. Sintering 40 (2008) 155–165.

[16] J. Rodríguez-Carvajal, Recent advances in magnetic structure determination by neutron powder diffraction, Phys. B 192 (1993) 55–69.

[17] E. Rodríguez, M.L. López, J. Campo, M.L. Veiga, C. Pico, Crystal and magnetic structure of the perovskites La_2MTiO_6 (M = Co, Ni), J. Mater. Chem. 12 (2002) 2798–2802.

[18] W.Z. Yang, X.Q. Liu, Y.Q. Lin, X.M. Chen, Structure, magnetic, and dielectric properties of $La_2Ni(Mn_{1-x}Ti_x)O_6$ ceramics, J. Appl. Phys. 111 (2012) 084106.

[19] I.G. de Muro, M. Insausti, L. Lezama, J.L. Pizarro, M.I. Arriortua, T. Rojo, Structural, Spectroscopic, Magnetic and Thermal Properties in the $[SrM(C_3H_2O_4)_2(H_2O)_5]\cdot 2H_2O$ (M = Mn, Fe, Co, Ni) System: Precursors of $SrMO_{3-x}$ Mixed Oxides, Eur. J. Inorg. Chem. 1999 (1999) 935–943.

[20] E. Rodríguez, I. Álvarez, M.L. López, M.L. Veiga, C. Pico, Structural, Electronic, and Magnetic Characterization of the Perovskite $LaNi_{1-x}Ti_xO_3$ ($0 \le x \le 1/2$), J. Solid State Chem. 148 (1999) 479–486.

[21] M. Yang, L. Huo, H. Zhao, S. Gao, Z. Rong, Electrical properties and acetone-sensing characteristics of $LaNi_{1-x}Ti_xO_3$ perovskite system prepared by amorphous citrate decomposition, Sens. Actuators, B 143 (2009) 111–118.

[22] C. Arrivé, T. Delahaye, O. Joubert, G. Gauthier, Exsolution of nickel nanoparticles at the surface of a conducting titanate as potential hydrogen electrode material for solid oxide electrochemical cells, J. Power Sources 223 (2013) 341–348.

[23] L. Kundakovic, M. Flytzani-Stephanopoulos, Reduction Characteristics of Copper Oxide in Cerium and Zirconium Oxide Systems, Appl. Catal., A 171 (1998) 13–29.

[24] Y.-S. Seo, A. Shirley, S.T. Kolaczkowski, Evaluation of thermodynamically favorable operating conditions for production of hydrogen in three different reforming technologies, J. Power Sources 108 (2002) 213–225.

Table 1. Hydrogen uptake, QPA, reduction degree of Ni^{2+} and Co^{2+} to Ni^{0}-Co^{0} or Ni^{2+} to Ni^{0} (LNTO) and average crystallite size of the prepared samples after TPR.

Sample	H_2 uptake (mol H_2 g^{-1})	Crystalline phases	QPA (%)	Reduction degree (%)		$^{c}L_{Ni^{0}\text{-}Co^{0}}$ (nm)
				^{a}TPR	^{b}QPA	
$LNT_{0.9}Co_{0.1}O$	$^{d}1.249$ x 10^{-3}	La_2TiO_5	22.60(0.65)	^{d}54.7	80.8	41
	$^{e}1.538$ x 10^{-3}	Ni^{0}-Co^{0}	10.88(0.54)	^{e}67.3		
		La_2O_3	18.82(0.54)			
		$La_2NiTi_{0.9}Co_{0.1}O_6$ non-s	47.70(1.03)			
$LN_{0.9}Co_{0.1}TO$	$^{d}9.219$ x 10^{-4}	La_2TiO_5	53.04(1.18)	^{d}44.3	86.7	42.3
	$^{e}1.165$ x 10^{-3}	Ni^{0}-Co^{0}	10.59(0.52)	^{e}56.0		
		La_2O_3	4.24(0.39)			
		$La_2Ni_{0.9}Co_{0.1}TiO_6$ non-s	32.13(0.86)			
LNTO	$^{d}8.962$ x 10^{-4}	La_2TiO_5	63.38(1.21)	^{d}43	97.1	31.1
	$^{e}1.376$ x 10^{-3}	Ni^{0}	11.87(0.53)	^{e}66.1		
		La_2O_3	1.82(0.26)			
		La_2NiTiO_6 non-s	22.93(0.78)			

Reduction degree calculated from ^{a}TPR results and ^{b}QPA obtained by means of Rietveld refinement.

^{c}In the case of LNTO, the average crystallite size $L_{Ni^{0}\text{-}Co^{0}}$ is changed by $L_{Ni^{0}}$.

The hydrogen uptake and the reduction degree are calculated by integration of the ^{d}second reduction peak (Fig. 2a) and ^{e}total isothermal period at 1000 °C (Fig. 2b) from TPR profiles.

The numbers in parentheses represent the standard deviation of the respective value.

Figure Captions

Figure 1. TPR of the as-synthesized materials from room temperature up to 1000 °C (the isothermal period at 1000 °C for 330 min is shown in the upper part).

Figure 2. Observed (orange symbols), calculated (black line) and difference (blue line) XRD profiles of (a) $LNT_{0.9}Co_{0.1}O$, (b) $LN_{0.9}Co_{0.1}TO$ and (c) LNTO after TPR. Vertical green bars indicate reflections of each crystalline phase.

Figure 3. (a) Methane conversion and (b) H_2/CO molar ratio evolution during steam reforming of methane over (■) $LNT_{0.9}Co_{0.1}O$, (○) $LN_{0.9}Co_{0.1}TO$ and (▲) LNTO.

Figure 1

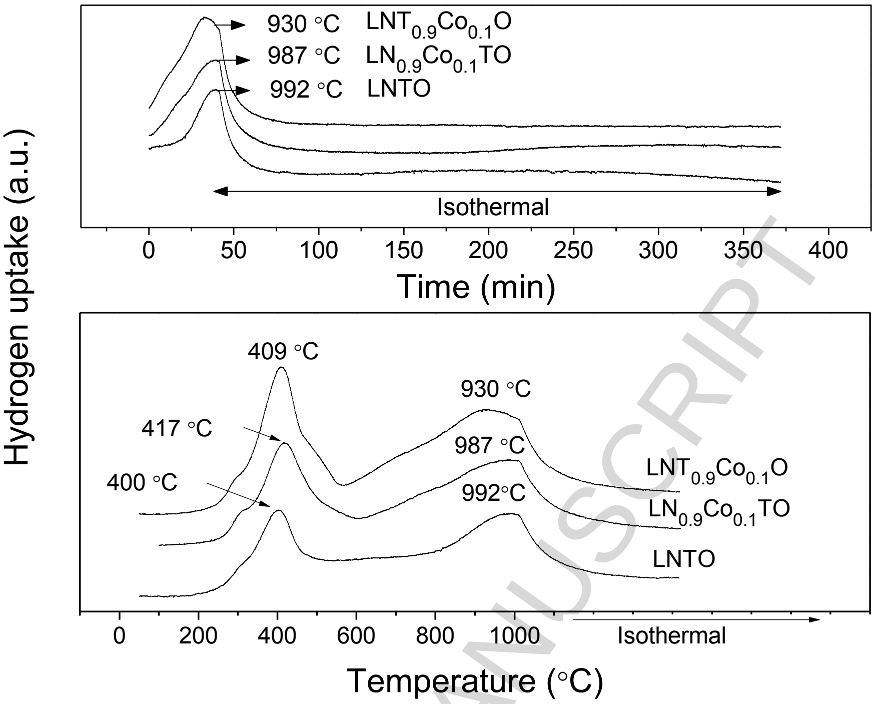
930 °C LNT$_{0.9}$Co$_{0.1}$O
987 °C LN$_{0.9}$Co$_{0.1}$TO
992 °C LNTO
Isothermal
0
50
100
150
200
250
300
350
400
Time (min)
Hydrogen uptake (a.u.)
409 °C
930 °C
417 °C
987 °C
400 °C
992°C
LNT$_{0.9}$Co$_{0.1}$O
LN$_{0.9}$Co$_{0.1}$TO
LNTO
0
200
400
600
800
1000
Isothermal
Temperature (°C)

Figure 2

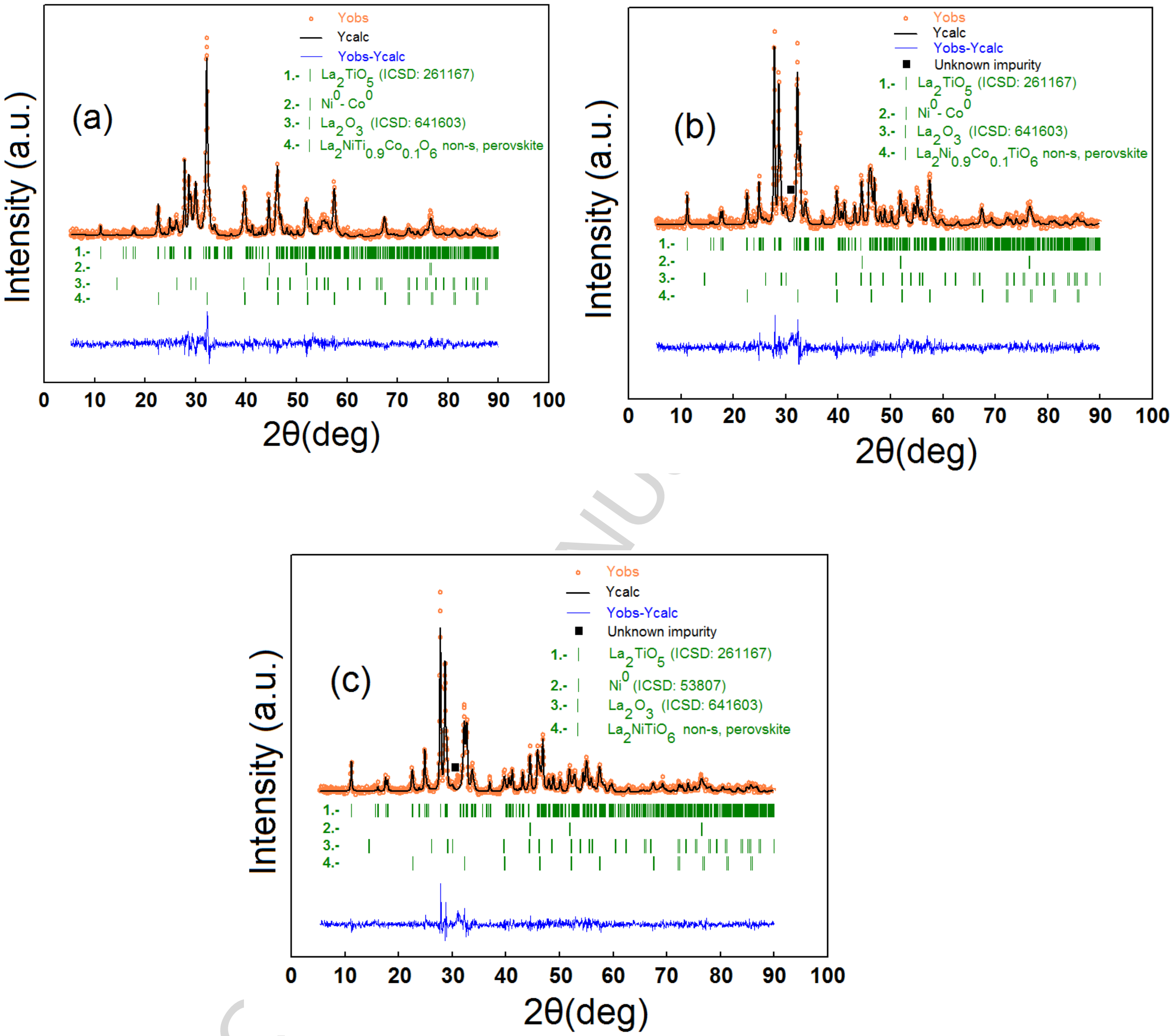
(a)
Yobs
Ycalc
Yobs-Ycalc
1.- | La2TiO5 (ICSD: 261167)
2.- | Ni0 - Co0
3.- | La2O3 (ICSD: 641603)
4.- | La2NiTi0.9Co0.1O6 non-s, perovskite
Intensity (a.u.)
2θ(deg)
0 10 20 30 40 50 60 70 80 90 100
(b)
Yobs
Ycalc
Yobs-Ycalc
Unknown impurity
1.- | La2TiO5 (ICSD: 261167)
2.- | Ni0 - Co0
3.- | La2O3 (ICSD: 641603)
4.- | La2Ni0.9Co0.1TiO6 non-s, perovskite
Intensity (a.u.)
2θ(deg)
0 10 20 30 40 50 60 70 80 90 100
(c)
Yobs
Ycalc
Yobs-Ycalc
Unknown impurity
1.- | La2TiO5 (ICSD: 261167)
2.- | Ni0 (ICSD: 53807)
3.- | La2O3 (ICSD: 641603)
4.- | La2NiTiO6 non-s, perovskite
Intensity (a.u.)
2θ(deg)
0 10 20 30 40 50 60 70 80 90 100

Figure 3

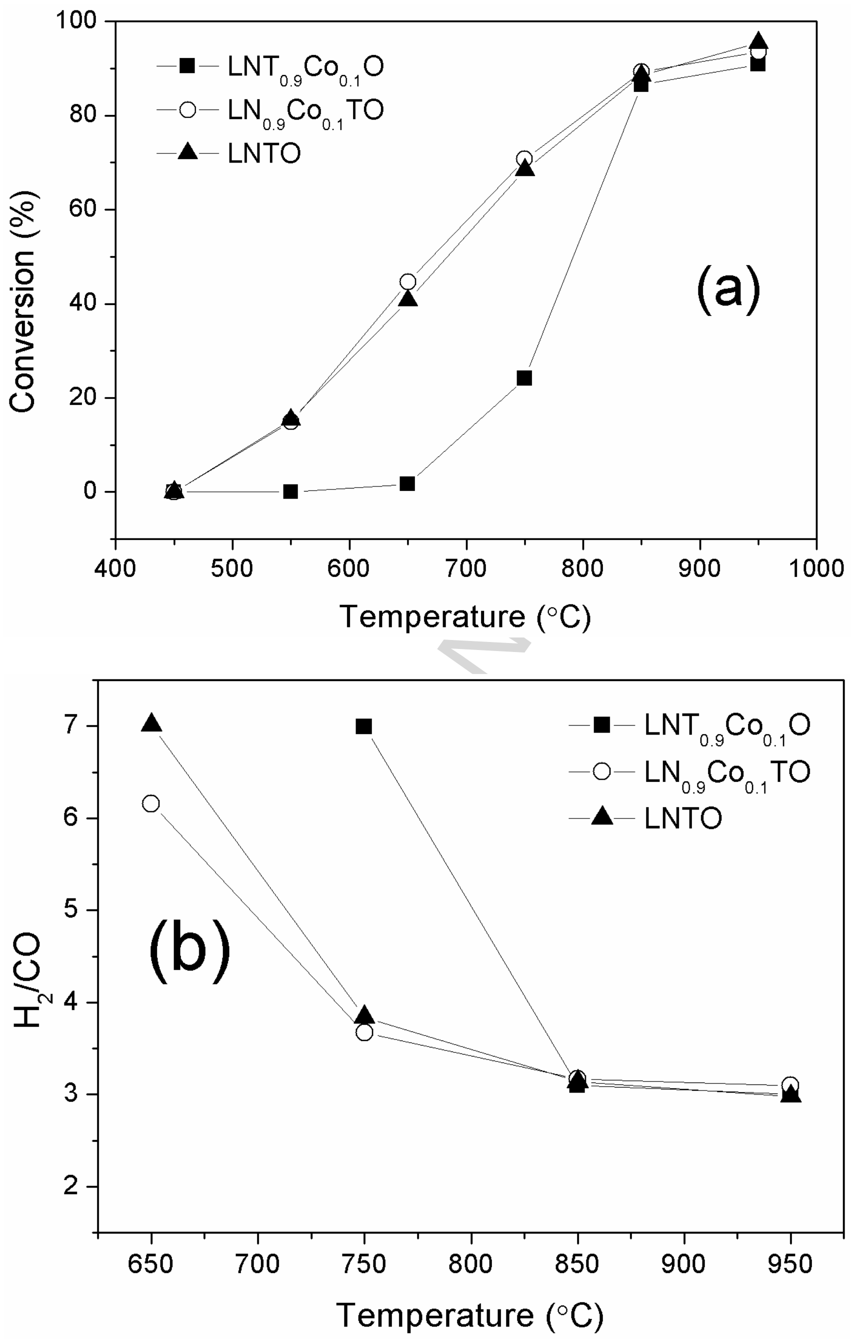
(a)
Conversion (%)
100
80
60
40
20
0
400
500
600
700
800
900
1000
Temperature (°C)
$LNT_{0.9}Co_{0.1}O$
$LN_{0.9}Co_{0.1}TO$
LNTO
(b)
H_2/CO
7
6
5
4
3
2
650
700
750
800
850
900
950
Temperature (°C)
$LNT_{0.9}Co_{0.1}O$
$LN_{0.9}Co_{0.1}TO$
LNTO

Graphical abstract

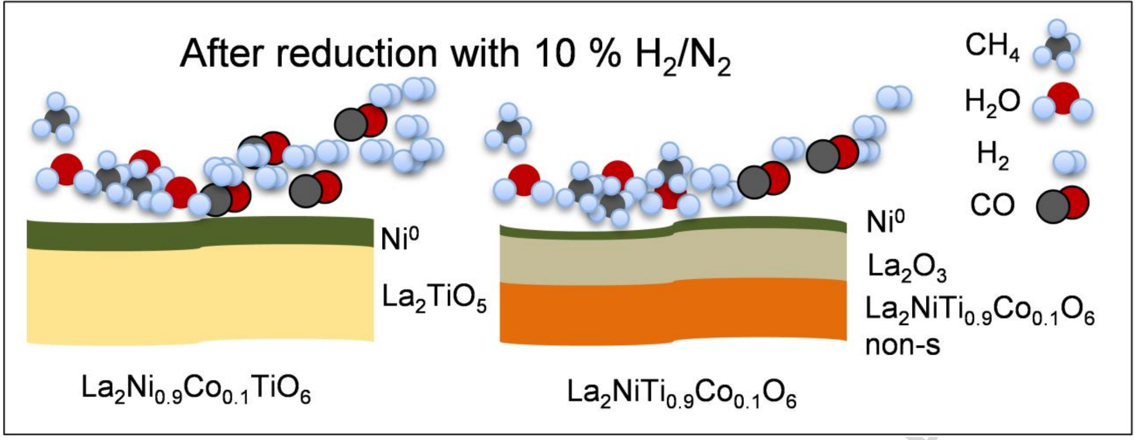

Highlight

- Ti^{4+} or Ni^{2+} from La_2NiTiO_6 double perovskite was partially substituted by Co^{2+}.
- Co^{2+} was included in the crystal structure of La_2NiTiO_6.
- After reduction at 1000°C the perovskite structure is partially decomposed.
- Activity on steam reforming of methane depends on reduction degree.